LLNL-JRNL-422323

Controlled incorporation of mid-to-high Z transition metals in CVD diamond

M. M. Biener, J. Biener, S. O. Kucheyev, Y. M. Wang, B. El-Dasher, N. E. Teslich, A. V. Hamza, H. Obloh, W. Mueller-Sebert, M. Wolfer, T. Fuchs, M. Grimm, A. Kriele, C. Wild

January 11, 2010

Diamond and related materials

Disclaimer

This document was prepared as an account of work sponsored by an agency of the United States government. Neither the United States government nor Lawrence Livermore National Security, LLC, nor any of their employees makes any warranty, expressed or implied, or assumes any legal liability or responsibility for the accuracy, completeness, or usefulness of any information, apparatus, product, or process disclosed, or represents that its use would not infringe privately owned rights. Reference herein to any specific commercial product, process, or service by trade name, trademark, manufacturer, or otherwise does not necessarily constitute or imply its endorsement, recommendation, or favoring by the United States government or Lawrence Livermore National Security, LLC. The views and opinions of authors expressed herein do not necessarily state or reflect those of the United States government or Lawrence Livermore National Security, LLC, and shall not be used for advertising or product endorsement purposes.

Controlled incorporation of mid-to-high Z transition metals in CVD diamond

M.M. Biener, J. Biener*, S.O. Kucheyev, Y.M. Wang, B. El-Dasher, N.E. Teslich, and A.V. Hamza

Nanoscale Synthesis and Characterization Laboratory, Lawrence Livermore National Laboratory, Livermore, CA 94550, USA

H. Obloh, W. Mueller-Sebert, M. Wolfer, T. Fuchs, M. Grimm, A. Kriele, and C. Wild

Fraunhofer-Institut für Angewandte Festkörperphysik, Tullastraße 72, 79108 Freiburg, Germany

*To whom correspondence should be addressed. E-mail: biener2@llnl.gov

Abstract

We report on a general method to fabricate transition metal related defects in diamond. Controlled incorporation of Mo and W in synthetic CVD diamond was achieved by adding volatile metal precursors to the diamond chemical vapor deposition (CVD) growth process. Effects of deposition temperature, grain structure and precursor exposure on the doping level were systematically studied, and doping levels of up to 0.25 at.% have been achieved. The metal atoms are uniformly distributed throughout the diamond grains without any indication of inclusion formation. These results are discussed in context of the kinetically controlled growth process of CVD diamond.

I. Introduction

Recently, diamond and its defect centers have received much interest in the fields of solid-state quantum computing[1-3], nanoscale magnetic sensor applications [4], and inertial confinement fusion where diamond is emerging as a promising ablator material [5-7]. In the latter application, the controlled incorporation of transition metals in diamond offers an opportunity to tailor diamond's x-ray adsorption properties to reduce preheating of the deuterium-tritium fuel and limit the growth of hydrodynamic instabilities [8]. In contrast to the quantum computing application, this requires relatively high mid-to-high atomic number (Z) doping levels in excess of one-tenth of an atomic percent. Unfortunately, diamond's high atomic density makes the incorporation of these larger atoms difficult. On the other hand, the principal possibility to incorporate larger metal atoms is demonstrated by the observation that diamond grown by high pressure-high temperature (HPHT) [9-12] or hot filament CVD (HFCVD) [13-18] methods commonly contains metal impurities from the catalyst (Ni, Co, Fe) or the filament material (W, Re, Ta). For the microwave plasma (MP) CVD technique, the incorporation of Mo impurities from the substrate holder has been reported [19].

Here, we describe a general approach to introduce transition metal related defect centers in diamond films grown by the microwave plasma CVD technique. Specifically, we report on the incorporation of Mo and W with controlled doping levels of up to 0.25 at.%, and discuss our results in context of the kinetically controlled growth process of CVD diamond. Controlled in-situ doping of CVD diamond with low-Z elements such as B, N, P, and S can be readily achieved by adding volatile precursor species during the CVD growth process [20-22]. We demonstrate that this approach can be extended to mid-to-high Z transition metals. Mo and W were selected due to the availability of volatile precursor species (hexa-carbonyls, $M(CO_6)$) that are compatible with the CVD diamond growth process.

Also, both metals form strong metal-carbon bonds which help to stabilize adsorbed precursor species during the high growth temperatures of CVD diamond (625-1100 ^{o}C). Furthermore, neither Mo or W are known to catalyze the graphitization of diamond.

2. Experimental

Metal doped CVD diamond films were grown in an ellipsoidal microwave plasma reactor[23] by adding volatile metal carbonyl precursors to the CH_4/H_2 feed gas. Typical growth conditions were 1-2% CH_4, 110-150 mbar, and 625-1100 °C. The thickness of the metal doped CVD diamond films was typically in the range of 3-10 microns, and the growth rates were in the 0.2-2 micron/h range depending on the actual deposition conditions. The majority of experiments were carried out on Mo doping, but very similar results were also obtained for W. For substrates, we used several μm thick polycrystalline diamond films grown on 3-inch diameter (001) Si wafers, both polished and as-grown. In some experiments, nitrogen was added to the CH_4/H_2 plasma to promote the formation of nanocrystalline material [24]. Wafer rotation was used to avoid angular non-uniformities arising from the gas flow. We also grew single crystalline metal-doped diamond films by using single crystalline natural diamond substrates with (111), (110), and (100) orientations, and their single crystalline character was verified by electron backscatter diffraction (EBSD). The metal precursors ($Mo(CO)_6$ and $W(CO)_6$) were delivered from a thermally stabilized source using H_2 as a carrier gas, and the precursor mole fraction in the plasma chamber was controlled by regulating the flow rate of the carrier gas (0-150 sccm) as well as the source temperature (298-318 K). The saturation vapor pressure of $Mo(CO)_6$ [25; 26] ($W(CO)_6$ [27]) in the source increases from 0.2 (0.03) mbar at 298 K to 1.4 (0.2) mbar at 318 K. For sample characterization, freestanding diamond wafers were prepared by removing the Si substrate using a hot KOH etch solution. From each wafer, several 5 x 5 mm^2 test samples were cut out from different

positions across the wafer by laser machining, and carefully cleaned by using chromsulfuric acid and HNO_3/HF followed by rinsing with acetone and methanol.

The dopant depth distribution was determined by secondary ion mass spectroscopy (SIMS) depth profile analysis using a 5 keV / 200-300 nA primary O_2^+ ion beam and a 200 x 200 μm^2 sputter area (only 25% of this area was used for analysis); the SIMS yield was calibrated against Rutherford backscattering spectroscopy (RBS, 2.0 MeV $^4He^+$ ions, scattering angle of 164°) using the RUMP code [28]. The phase purity of our metal doped diamond films was checked by glancing angle X-ray diffraction (GAXRD) analysis (CuKα_1 line, incidence angle fixed at 2°) and Raman spectroscopy (backscattering geometry, 457.9 nm, spot size of 200 μm). GAXRD was also used to check for the presence of metal or metal carbide inclusions. The surface morphology was assessed by scanning electron microscopy (SEM) or optical microscopy, and the films typically exhibited a well-faceted polycrystalline morphology (with exception of the single crystal films which exhibited a relatively smooth surface morphology). The film microstructure was studied by high angle annular dark field (HAADF) scanning transmission electron microscopy (STEM) and bright-field (BF) TEM using a Philips CM300FEG instrument operating at 300 kV. TEM cross sections were prepared using the focused ion beam (FIB) lift out technique. The microscopic structure of the metal centers was investigated by RBS/channeling. Cross-sectional radiographs (XRT XuM system, 20 kV x-ray point source, Pt Lα line at 9.9441 keV) were obtained to demonstrate the effect of metal incorporation on the x-ray adsorption behavior.

3. Results and Discussion

3.1 Doping level and dopant distribution

The ability to grow several micron thick Mo-doped diamond films with a substantially uniform doping profile by adding $Mo(CO)_6$ to the CVD diamond process is demonstrated by the SIMS depth profile shown in Figure 1a. The Mo depth distribution is fairly uniform with a concentration of ~0.25 at%. To check for lateral uniformity, RBS spectra were collected from various points across the wafer. The Mo distribution was found to be axially symmetric but radially non-uniform with the highest Mo concentration at the wafer edge (5-10 times higher than at the wafer center). This indicates transport limitations and depletion of the metal precursor by the gas phase decomposition.

To study effects of the grain structure, deposition temperature and precursor exposure on the doping level, we systematically varied deposition parameters including source temperature, flow rate of the carrier gas and total pressure. The most important parameter in controlling the metal doping level seems to be the deposition temperature. Specifically, we found that the doping level increases by more than one order of magnitude, from ~0.01 to ~0.25 at.%, by decreasing the deposition temperature from 1100 ^{o}C to 625 ^{o}C. (Figure 1b). For any given temperature, the doping level can be increased by increasing the precursor mole fraction in the plasma chamber until the maximum doping level for that temperature is reached (these are the doping levels shown in Figure 1b). Increasing the precursor exposure beyond this point can lead to deposition of a thin metal/metal carbide film on top of the growing diamond film without further increasing the doping level of the diamond film underneath. Surprisingly, the formation of this metal/metal carbide film did not seem to suppress the growth of the underlying diamond film as judged by the experimentally observed average growth rate. The observed temperature dependence suggests that the doping level is predominantly controlled by the precursor life time under growth conditions.

On the other hand, the doping level seems to be rather insensitive to the specific grain structure or defect density of the deposited material. Polycrystalline and single crystalline (marked 'sc' in Figure 1b) diamond films grown under otherwise identical conditions showed comparable doping levels. For example, the Mo doping level of single crystalline (<111>, <110>, <100>) and polycrystalline diamond films grown simultaneously at 630 °C was found to vary only very little between 0.20 (<111> and <110>) and 0.25 at.% (polycrystalline). Furthermore, adding nitrogen to the CH_4/H_2 feed gas, which is known to reduce the grain size of the deposited material, did not affect the doping level at a given deposition temperature. Interestingly, we observed that doped films that were deposited under conditions which normally would result in the formation of nanocrystalline material, still showed an ultrafine-grained film morphology. Metal incorporation thus seems to improve the crystallinity of CVD diamond films, a phenomenon which has also been reported for metal impurities in HFCVD diamond films [16].

All these observations suggest that the incorporated Mo/W atoms are not associated with grain boundaries or defects but are uniformly distributed throughout the film. Furthermore, the incorporation of Mo and W atoms from their hexacarbonyl precursor molecules seems to be almost independent of the specific surface chemistry as demonstrated by the single crystal experiments. This is a surprising result in view of the pronounced impurity level/growth sector dependence generally observed for synthetic diamond. For example, boron and nitrogen impurities in CVD diamond are preferentially incorporated in the {111} growth sector, and the impurity level found in the {100} growth sector is lower by at least a factor of three [29-31]. Similarly, Ni impurities in HPHT diamond have been found to be concentrated in {111} growth sectors [10].

3.2 Phase verification

The phase purity of our transition metal doped diamond films was verified by GAXRD analysis. Figure 2 shows GAXRD spectra obtained from highly Mo (0.25 at.%) and W (0.22 at.%) doped diamond films. Only diffractions peaks which can be attributed to the diamond phase are observed thus ruling out the formation of transition metal or metal carbide micro-inclusions which previously have been reported for diamond grown by HFCVD [14] and HPHT [12] methods.

Additionally, Raman measurements were carried out to assess the quality of the metal doped diamond films and to check for the presence of non-crystalline carbon phases (Figure 3). The Raman spectra of both Mo and W doped diamond films are dominated by a sharp line at 1332 cm^{-1} characteristic for high quality diamond films [32-34]. The fact that the line position does not shift upon metal doping suggests that incorporation of large transition metal atoms in the diamond lattices does not lead to compressive stress build-up. The weak scattering in the 1450 – 1600 cm^{-1} region, which is more pronounced for the Mo doped sample, indicates the presence of some non-diamond carbon.

3.3. Film microstructure

The distribution of Mo in highly Mo-doped diamond films was further studied by HAADF-STEM, BF TEM, and area-selective EDX analysis (Figure 4). We found no indication of defect or grain boundary enrichment. This observation is consistent with our XRD results and further rules out the presence of inclusions of transition metal carbides. In our case, the incorporated Mo seems to be uniformly distributed throughout the grains of the Mo-doped diamond film. This conclusion was further confirmed by an area-selective EDX analysis (data not shown). However, doping seems to increase the defect density within the grains. The TEM images shown in Figure 4 also demonstrate that the interface between doped and undoped regions of the diamond is smooth and well defined.

3.4 Metal center structure

To probe the lattice site location of Mo, we performed RBS/channeling experiments on single crystalline Mo-doped diamond samples (Figure 5). The observed angular dependence reveals that Mo does not reside on substitutional or tetrahedral interstitial sites in the cubic diamond lattice. Mo and W are probably simply too big to fit into these sites as the atomic volume of Mo and W is roughly three times that of carbon (~5.7 $Å^3$) in diamond. Most likely, more complex sites are formed such as the metal-vacancy clusters which have been suggested for Ni impurities [9; 35]. Here, the metal atom displaces more than one carbon atom in the lattice, whereby relieving compressive strain around the larger impurity atoms.

3.5 *X-ray adsorption properties*

To demonstrate the effect of metal incorporation on the x-ray adsorption behavior of diamond for the ICF application, we collected cross-sectional radiographs from a highly Mo doped (0.2 at. %) diamond film (Figure 6). The contrast produced by Mo doping is very uniform, consistent with the uniform distribution of metal atoms revealed by TEM. The sharp interface between doped and undoped regions of the diamond film also demonstrates that the metal atoms are not mobile at the deposition temperature (630 ^{o}C in this example).

4. Conclusions

The incorporation of large transition metal atoms into the dense diamond lattice can be understood in context of the kinetically controlled growth mode of CVD diamond films. At first glance, incorporation of large metal atoms such as Mo or W into the dense diamond lattice seems to be difficult, but one has to

remember that their incorporation into the growing diamond film does not necessarily require the displacement of several carbon atoms (which requires breaking of C-C bonds and vacancy diffusion) nor the build-up of large compressive stresses. The metal atoms adsorbed on the growth surface can simply be incorporated by being overgrown by diamond thus replacing one or more carbon atoms in the growing diamond film depending on the size of the metal atom. Note that a so-formed metal center is equivalent to a metal-vacancy cluster formed by capture of migrating vacancies by an interstitial/substitutional metal atom. In this scenario, the probability of metal incorporation is kinetically controlled by the competition between metal precursor desorption (metal precursor residence time) and diamond growth rate thus explaining the observed temperature dependence. Surface diffusion does not seem to play a major role as this should result in metal decoration of defects such as grain boundaries and/or metal carbide precipitate formation. In this model, a strong metal-carbon bond helps to achieve high doping levels (increasing the precursor residence time), and to prevent defect decoration and/or metal precipitation (limiting the surface mobility). If, on the other hand, the metal atoms would be incorporated by thermal diffusion and vacancy capture, the process would require a high density of vacancies. For example, the stress-neutral incorporation of Mo or W would require that the vacancy density is three times the atomic density of the incorporated metal atoms, or 1.33×10^{21} vacancies/cm^3 for 0.25 at.% Mo/W.

In summary, we have developed a simple approach that allows one to grow uniform metal doped CVD diamond films with well-defined doping levels up to ~0.25 at.% and sharp interfaces between doped and undoped regions. The approach described here is universal in nature, and can be applied to other transition metals forming strong metal-carbon bonds. Moreover, our approach offers a new operating window for controlled generation of metal related defect structures in diamond as it is not

limited by thermodynamics (as the HPHT process) or to metals which can be used as filament material (HFCVD).

Work at LLNL was performed under the auspices of the U.S. DOE by LLNL under Contract DE-AC52-07NA27344.

References:

[1] S. Prawer, A.D. Greentree, Science 320 (2008) 1601.

[2] D.A. Simpson, E. Ampem-Lassen, B.C. Gibson, S. Trpkovski, F.M. Hossain, S.T. Huntington, A.D. Greentree, L.C.L. Hollenberg, S. Prawer, Appl. Phys. Lett. 94 (2009) 203107.

[3] J.R. Rabeau, Y.L. Chin, S. Prawer, F. Jelezko, T. Gaebel, J. Wrachtrup, Appl. Phys. Lett. 86 (2005) 131926.

[4] J.M. Taylor, P. Cappellaro, L. Childress, L. Jiang, D. Budker, P.R. Hemmer, A. Yacoby, R. Walsworth, M.D. Lukin, Nat. Phys. 4 (2008) 810.

[5] J. Biener, et al., Fusion Sci. Technol. 49 (2006) 737.

[6] M.D. Knudson, M.P. Desjarlais, D.H. Dolan, Science 322 (2008) 1822.

[7] J. Biener, et al., Nucl. Fusion 49 (2009) 112001.

[8] R.C. Cook, et al., Laser Part. Beams 26 (2008) 479.

[9] A.T. Collins, Diamond Relat. Mater. 9 (2000) 417.

[10] Y. Meng, M. Newville, S. Sutton, J. Rakovan, H.K. Mao, Am. Mineral. 88 (2003) 1555.

[11] V.A. Nadolinny, J.M. Baker, O.P. Yuryeva, M.E. Newton, D.J. Twitchen, Y.N. Palyanov, Appl. Magn. Reson. 28 (2005) 365.

[12] H. Sumiya, N. Toda, S. Satoh, SEI Technical Review 60 (2005) 10.

[13] J. Cifre, F. Lopez, J.L. Morenza, J. Esteve, Diamond Relat. Mater. 1 (1992) 500.

[14] E. Gheeraert, A. Deneuville, M. Brunel, J.C. Oberlin, Diamond Relat. Mater. 1 (1992) 504.

[15] M. Griesser, G. Stingeder, M. Grasserbauer, H. Baumann, F. Link, P. Wurzinger, H. Lux, R. Haubner, B. Lux, Diamond Relat. Mater. 3 (1994) 638.

[16] P.M. Menon, A. Edwards, C.S. Feigerle, R.W. Shaw, D.W. Coffey, L. Heatherly, R.E. Clausing, L. Robinson, D.C. Glasgow, Diamond Relat. Mater. 8 (1999) 101.

[17] H.F. Winters, H. Seki, R.R. Rye, M.E. Coltrin, J. Appl. Phys. 76 (1994) 1228.

[18] F. Jansen, M.A. Machonkin, D.E. Kuhman, J. Vac. Sci. Technol. A 8 (1990) 3785.

[19] A. Kromka, R. Kravetz, A. Poruba, J. Zemek, V. Perina, J. Rosa, M. Vanecek, Phys. Stat. Sol. A 199 (2003) 108.

[20] R. Haubner, Diamond Relat. Mater. 14 (2005) 355.

[21] M. Nesladek, Semicond. Sci. Technol. 20 (2005) R19.

[22] M. Nesladek, D. Tromson, P. Bergonzo, P. Hubik, J.J. Mares, J. Kristofik, D. Kindl, O.A. Williams, D. Gruen, Diamond Relat. Mater. 15 (2006) 607.

[23] M. Füner, C. Wild, P. Koidl, Appl. Phys. Lett. 72 (1998) 1149.

[24] C.J. Tang, A.J. Neves, S. Pereira, A.J.S. Fernandes, J. Grácio, M.C. Carmo, Diamond Relat. Mater. 17 (2008) 72.

[25] W.C.J. Wei, M.H. Lo, Appl. Organomet. Chem. 12 (1998) 201.

[26] T. Ohta, F. Cicoira, P. Doppelt, L. Beitone, P. Hoffmann, Chemical Vapor Deposition 7 (2001) 33.

[27] D. Chandra, K.H. Lau, W.-M. Chien, M. Garner, Journal of Physics and Chemistry of Solids 66 241.

[28] L.R. Doolittle, Nucl. Instrum. Meth. B 9 (1985) 344.

[29] T. Kolber, K. Piplits, R. Haubner, H. Hutter, Fresen. J. Anal. Chem. 365 (1999) 636.

[30] R. Locher, J. Wagner, F. Fuchs, M. Maier, P. Gonon, P. Koidl, Diamond Relat. Mater. 4 (1995) 678.

[31] R. Samlenski, C. Haug, R. Brenn, C. Wild, R. Locher, P. Koidl, Diamond Relat. Mater. 5 (1996) 947.

[32] D.S. Knight, W.B. White, J. Mater. Res. 4 (1989) 385.

[33] J. Wagner, C. Wild, P. Koidl, Appl. Phys. Lett. 59 (1991) 779.

[34] S.R. Sails, D.J. Gardiner, M. Bowden, J. Savage, D. Rodway, Diamond Relat. Mater. 5 (1996) 589.

[35] R. Larico, J.F. Justo, W.V.M. Machado, L.V.C. Assali, Physica B 376 (2006) 292.

Figure 1: Doping level and dopant distribution. a) Mo SIMS depth profile of a ~6-μm-thick Mo-doped diamond film grown at 630 ^{o}C. b) Dependence of the Mo (circles) and W (squares) incorporation level on the deposition temperature. Open symbols (□,○) indicate films (labelled 'air') which were grown in the presence of a controlled air leak (~ 1000 ppm N_2), and half filled symbols indicate films (labelled 'sc') grown on single crystal diamond substrates.

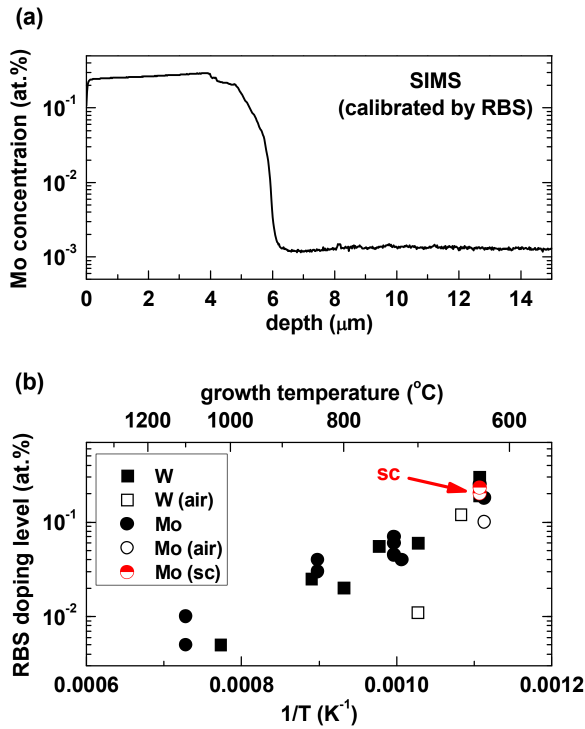

Figure 2: Glancing angle x-ray diffraction (GAXRD) spectra obtained from highly Mo (0.25 at.%) and W (0.22 at.%) doped diamond films grown at 630 ^{o}C. The incidence angle was fixed at 2°. The observed diffraction peaks can be attributed to the (111), (220), (311), (400) and (331) planes of the diamond lattice. No other graphite or Mo/W carbide related diffraction peaks are observed.

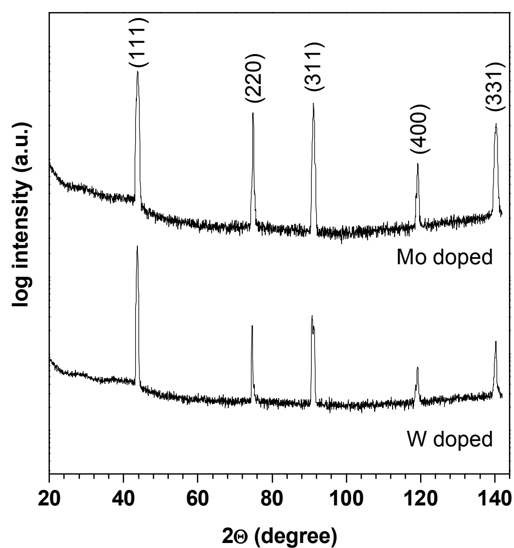

Figure 3: Raman spectra of Mo (0.25 at.%)and W (0.22 at.%) doped diamond films excited at 457.9 nm.

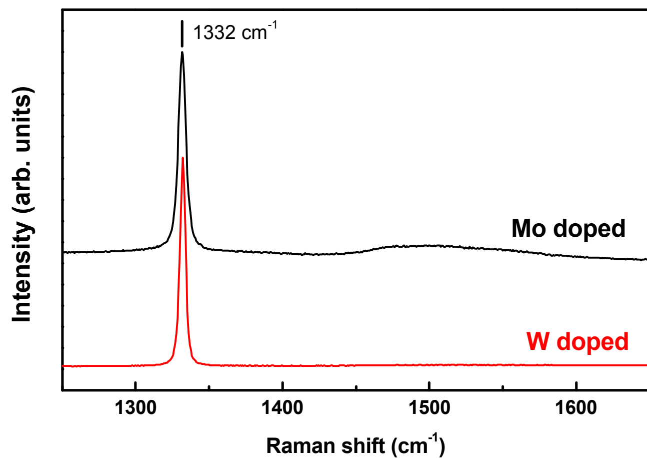

Figure 4: a) Cross-sectional HAADF STEM micrograph of a coarse grained Mo-doped diamond film grown at 630°C (Mo doping level ~0.25 at.%). Grain boundaries and the interface between doped and undoped material are indicated by GB and IF, respectively. (C marks the protective carbon layer used to reduce FIB damage). b) Higher magnification BF TEM image of the area within the box in Fig. 2a.

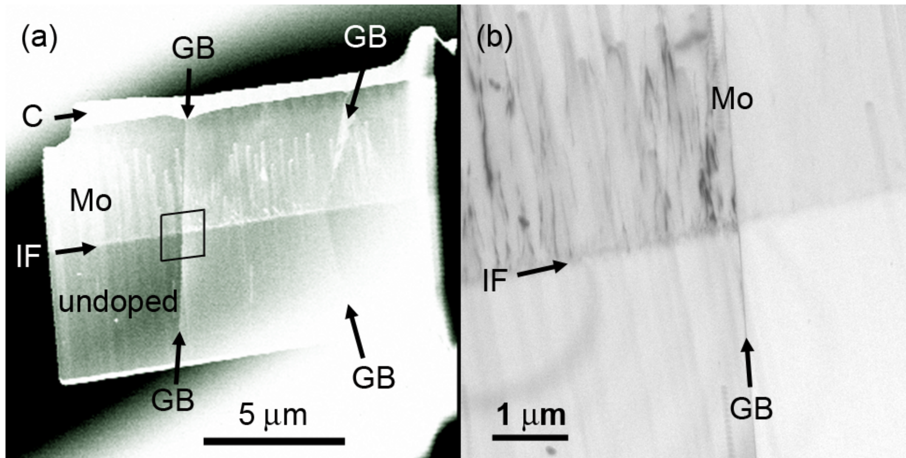

Figure 5: RBS/channeling data collected from a single crystalline Mo-doped diamond film (100 orientation). The angular dependence shown in the inset reveals that Mo does not reside on substitutional or tetrahedral interstitial sites.

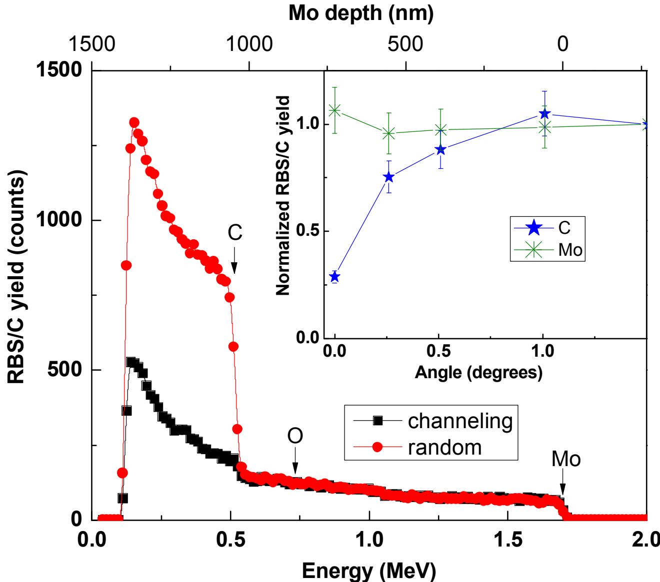

Figure 6: Cross-sectional radiograph of a wedge-shaped Mo-doped diamond sample (the thickness increases from top to bottom) demonstrating the effect of metal incorporation on the x-ray contrast. The thickness of the Mo-doped layer (doping level 0.2 at. %) is ~10 micron.